Thin Solid Films 518 (2010) S104–S112

Contents lists available at ScienceDirect

Thin Solid Films

journal homepage: www.elsevier.com/locate/tsf

Quest of electric field controlled spintronics in MnGe

Kang L. Wang *, Faxian Xiu

Device Research Laboratory, Department of Electrical Engineering, University of California, Los Angeles, California, 90095, USA

ARTICLE INFO

Available online 20 October 2009

Keywords:
Diluted magnetic semiconductors
Spintronics
MnGe
Quantum dots
Hole-mediated ferromagnetism

ABSTRACT

With the seemly limit of scaling on CMOS microelectronics fast approaching, spintronics has received enormous attention as it promises next generation nanometric magneto-electronic devices; particularly, the electric field control of ferromagnetic transition in dilute magnetic semiconductor systems offers the magneto-electronic devices a potential for low power consumption and low variability. In this paper, we first review the current efforts on the development of Mn-doped Ge (MnGe) magnetic materials, followed by an analysis of MnGe thin films grown by molecular beam epitaxy. Then we show that with zero and one dimension quantum structures, superior magnetic properties of MnGe compared with bulk films can be obtained. More importantly, we demonstrate a field controlled ferromagnetism in these MnGe nanostructures at 50 K. The controllability of ferromagnetism in this material system is a major step towards the Ge-based spintronic devices.

1. Introduction

International technology roadmap for semiconductors (ITRS) has outlined the needs of emerging materials and devices in order to meet the challenges of continued scaling of CMOS: energy dissipation and variability among others. [1] Ge-based diluted magnetic semiconductors (DMSs) have attracted extensive attention due to their possibility to be integrated with the mainstream Si microelectronics, in which Ge-based DMS may be used to enhance the functionality of Si integrated circuits [2]. In particular, the hole mediated effect discovered in Mn_xGe_{1-x} opens up tremendous possibilities to realize spintronic devices with advantages in reducing power dissipation in addition to increasing new functionalities, leading to perhaps normally off computers.

However, the growth of high-quality Mn_xGe_{1-x} DMS with high Curie temperature (T_c>300 K) presents a significant challenge. In most cases, it was often observed that the metallic clusters were developed inside MnGe thin films in a random and uncontrollable manner. The genuine MnGe DMS material typically had an extremely narrow growth window with poor reproducibility. Table 1 summarizes the current status of MnGe on the growth method, the Curie temperature, and the field controllability of ferromagnetism. Two categories are considered: MnGe thin films [3–11] and nanostructures [12–15]. Park et al. found that the Curie temperature of MnGe thin films increased linearly with Mn concentration from 25 to 116 K. The field controlled ferromagnetism was observed in a simple gated structure through application of a small gate voltage, showing a clear hole mediated effect at 50 K, which has attracted significant interest in MnGe research [3]. Later experiments aimed to further increase the Curie temperature and to obtain the electric field controllability at room temperature. Among these efforts, Cho et al. reported the synthesis of Mn-doped bulk Ge single crystals with 6% of Mn and a high ferromagnetic order at about 285 K. The origin of the high Curie temperature was found to be complex because of the presence of dilute and dense Mn-doped regions. [4] Other experiments have reported room temperature ferromagnetism by different growth methods, exclusively attributing to the presence of the metallic phases, Mn_5Ge_3 and $Mn_{11}Ge_8$ [6–11]. No field controlled ferromagnetism was reported. Recently, Jamet et al. reported that under a narrow growth window, another type of MnGe clusters, $MnGe_2$ could be developed with a ~33% of Mn with a Curie temperature beyond 400 K. [5] A remarkable feature of these clusters is the large magnetoresistance due to the formation of $MnGe_2$ nanocolumns. However, the poor reproducibility of $MnGe_2$ nanocolumns made it difficult to produce reliable spintronic devices. To date, there has been progress in producing pure MnGe DMS thin films [3,4,16–18]; however, the formation of uncontrollable metallic clusters yet remains a challenge [6–9,19]. High Curie temperature DMS thin films without any precipitations seem to be a major obstacle for the fabrications of any practical spintronic devices to function at room temperature.

In the next section, we discuss the progress in MnGe nanostructures. Recently, MnGe nanostructures such as MnGe nanowires were demonstrated to be single crystalline DMS with a Curie temperature beyond 300 K [12,13]. Unfortunately, the origin of the high temperature ferromagnetism is unknown although the existence of typical MnGe clusters clearly was clearly ruled out. Other nanostructures

* Corresponding author.
E-mail address: wang@ee.ucla.edu (K.L. Wang).

0040-6090/$ – see front matter © 2009 Elsevier B.V. All rights reserved.
doi:10.1016/j.tsf.2009.10.066

Table 1
A brief summary of MnGe thin film growth.

Mn-doped Ge	Growth method	Mn (%)	Tc (K)	Origin of FM	Field Controlled FM	Ref.
Mn-doped Ge thin films/bulk						
DMS	MBE	0.6~3.5	25~116	DMS	50 K	[3]
Bulk single crystal	Sintering	6.2	~285	Not clear	No	[4]
Metallic clusters	MBE	<6	~300	Mn_5Ge_3, $Mn_{11}Ge_8$	No	[6–9]
Ion implantation	Implantation	A few	~300	Mn_5Ge_3, $Mn_{11}Ge_8$	No	[10,11]
$MnGe_2$ clusters	MBE	6	>400	$MnGe_2$ clusters	No	[5]
Mn-doped Ge nanostructures						
Nanowires	Sintering; chemical synthesis	<20	>300	DMS	No	[12,13]
Quantum dots	Implantation	A few	230; 350	230 K: DMS 350 K: Mn_5Ge_3	No	[14]
Nanodots	Implantation	2	~340	DMS, Mn_5Ge_3, $Mn_{11}Ge_8$	10 K	[15]

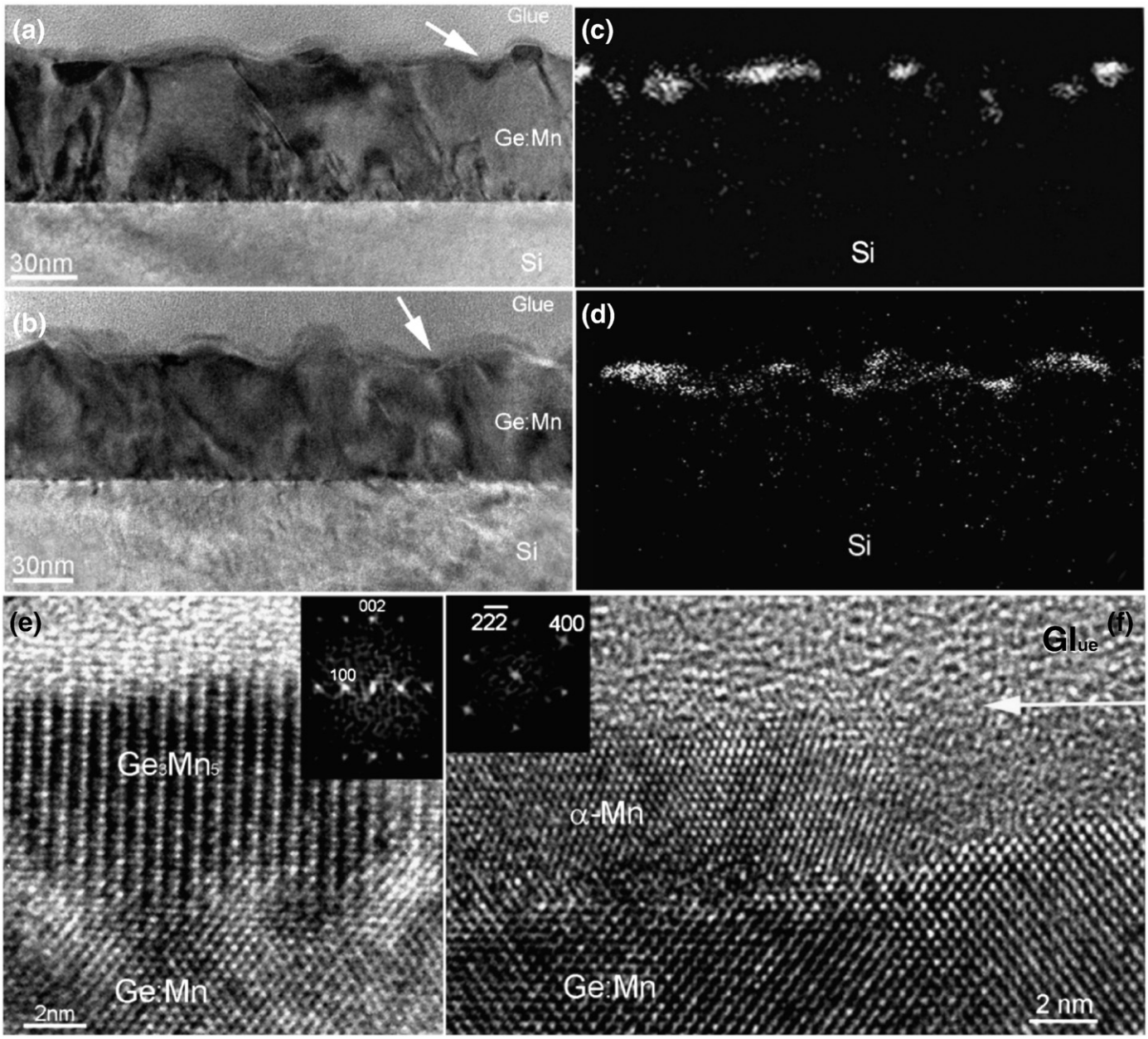

Fig. 1. (a) as-grown sample at 250 °C, (b) annealed sample at 400 °C; (c) and (d) are corresponding Mn maps of (a) and (b), respectively; (e) HR-TEM image of (a) typical Mn_5Ge_3 cluster; (f) HR-TEM image of a typical α-Mn metallic cluster epitaxially grown on the (Mn)Ge lattice. The insets in (e) and (f) are the corresponding FFT maps of the images.

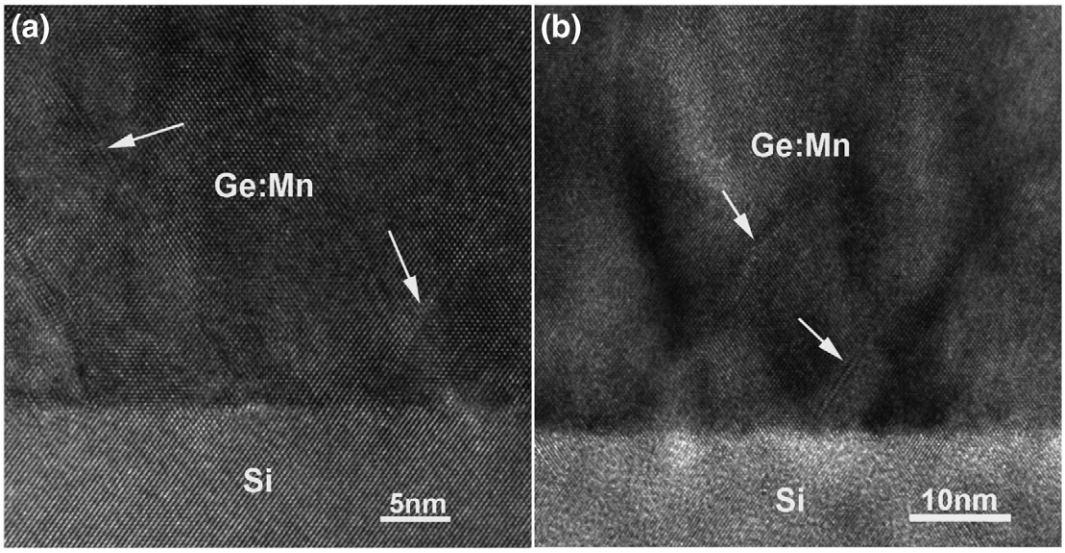

Fig. 2. 80 nm-thick Mn-doped Ge grown on Si at 250 °C, (a) as-grown film and (b) after 400 °C annealing at for 30 min. Stacking faults are marked by arrows.

involve the use of Mn ion implantation into Ge dots or Ge substrate. And the MnGe nanodots were successfully developed [14,15]. However, by using this method, the metallic clusters were observed, similar to the scenario of MnGe thin films. Thus, it is our presumption that the Mn doping behavior and magnetic properties are drastically different when the material dimension becomes smaller. Bulk MnGe films always tend to form clusters no matter what growth conditions are. When it comes to the one and zero dimensions, the cluster formation may be possibly limited because the Mn concentration cannot accumulate enough and the strain can be easily accommodated to minimize the metallic clusters when the material dimension becomes small [7,8].

In this paper, first we analyze structural and magnetic properties of typical MnGe thin films with different thickness grown by molecular beam epitaxy (MBE). Then we show that, with nanostructures (nanowires and quantum dots), MnGe DMS can be successfully produced. Then we describe the self-assembled MnGe DMS quantum dots grown by MBE, which have a high Curie temperature (T_c>400 K). Finally, we demonstrate a field controlled ferromagnetism in metal-oxide-semiconductor (MOS) structures using these quantum dots as the channel layers.

2. 80 nm-thick MnGe thin films by molecular beam epitaxy

Mn-doped Ge films were grown on Si substrates by a Perkin-Elmer solid source molecular beam epitaxy system. Si substrates were cleaned by H_2SO_4:H_2O_2 (5:3) and 10% HF with a final step of HF etching. The native oxide was removed by a 10 min flash at 800 °C in the vacuum chamber. After that, a direct growth of 80 nm-thick MnGe on Si were carried out at 250 °C. A 5 nm Ge capping layer was deposited on the surface in order to prevent MnGe from oxidizing. To understand the annealing effect, identical MnGe thin films were grown repeatedly and followed by *in-situ* annealing process at 400 °C for 30 min. All as-grown and annealed samples were characterized by high resolution transmission electron microscopy (HR-TEM, FEI Tecnai F30 operating at 200 keV) and superconducting quantum interference device (SQUID, Quantum Design MPMS XL 5). Cross-section HR-TEM specimens along ⟨110⟩ were prepared by using a tripod technique, followed by a final thinning using a Gatan precision ion polishing system.

Fig. 1(a) and (b) show cross-sectional TEM images of the as-grown and annealed 80 nm-thick $Mn_{0.04}Ge_{0.96}$. Non-uniform and discontinued rough films were observed in both cases. Fig. 1(c) and (d) are their corresponding Mn elemental maps, respectively. Mn is seen to concentrate on top for both samples. Mn-containing clusters are confirmed near the top of the crystalline layer as indicated by the white arrow in Fig. 1(a). A HR-TEM image clearly indicates that a Mn-containing cluster is formed on top of the Ge lattice as shown in Fig. 1(e). Using the lattice constant of Ge as the reference, the lattice spacings of the Mn-containing cluster can be determined as 0.62 and 0.25 nm, which are matched with the distances of (100) and (002) atomic planes of the hexagonal Mn_5Ge_3 phase. The fast Fourier transformation (FFT) map shown in the inset of Fig. 1(e) also indicates that the cluster belongs to the hexagonal Mn_5Ge_3 phase. Mn_5Ge_3 clusters may be formed when the Mn concentration is sufficiently high for the nucleation of clusters [7].

Fig. 2 shows the TEM cross-section of as-grown and 400 °C annealed samples. Stacking faults along {111} atomic planes are clearly observed in both cases. The annealing process does not dramatically affect the stacking-faults. However, the magnetic properties have a noticeable change. Fig. 3(a) and (d) show clear hysteresis loops at 298 K for both the as-grown and annealed samples. Before annealing, the film shows a clear hysteresis at 10 K while a very small magnetic moment is observed at room temperature. After annealing, the hysteresis showed a significant change and the coercive field at 10 K decreased from 430 Oe to 92 Oe. For the as-grown film, Mn_5Ge_3 formed on the surface gave the Curie temperature of around 298 K as shown in Fig. 3(b). The blocking temperature was estimated to be about 250 K. After annealing, both Mn_5Ge_3 and Mn clusters led to a complex magnetic behavior, showing multiple phase transitions at different temperatures in Fig. 3(e). The Curie temperature increased from 298 to over 400 K. Further investigation is needed to understand the change of the magnetic property. The Arrott's plots were made to confirm the Curie temperature in Fig. 3(c) and (f). The estimated Curie temperatures for the as-grown and annealed samples were obtained to be 298 K and above 400 K, respectively.

3. 15 nm-thick MnGe films by molecular beam epitaxy

To understand the behavior of Mn in an ultra-thin Ge, a MnGe film with a thickness of about 15 nm was grown directly on Si substrate by following the same growth procedure as that for the 80 nm-thick film. Fig. 4(a) and (b) show typical cross-sectional TEM images and general

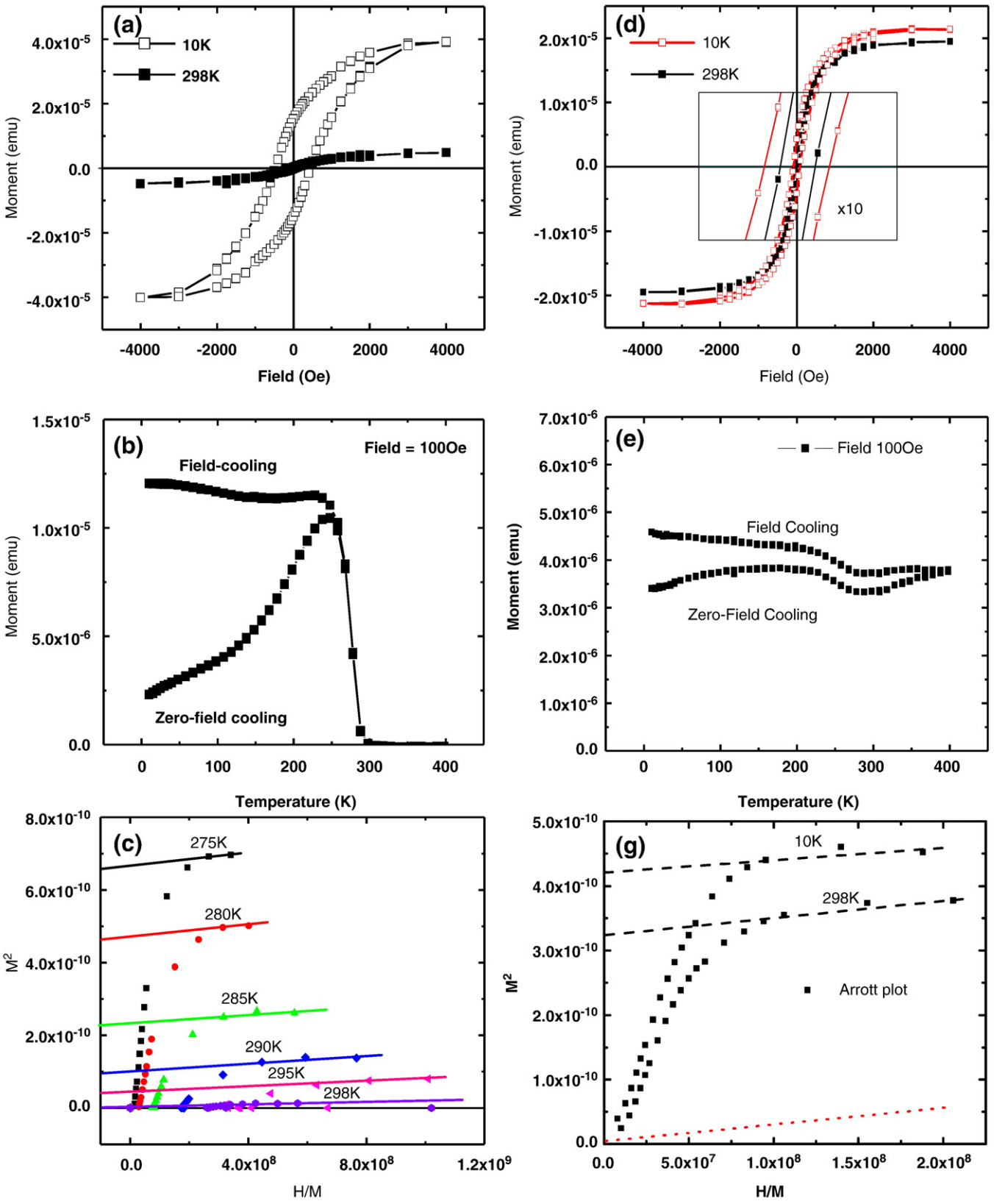

Fig. 3. SQUID measurement of 4% Mn-doped Ge grown on Si, the left column is for the as-grown film and the right column is the film after 400 °C annealing. (a) and (d) are the hysteresis loops at 10 and 298 K; (b) and (e) are moment versus temperature curves; (c) and (f) are Arrott's plots. The red line in (f) shows the expected Arrott's plot at the Curie temperature. (For interpretation of the references to colour in this figure legend, the reader is referred to the web version of this article.)

morphologies of the as-grown and annealed samples. From these figures, a relative uniform crystalline layer, adjacent to the Si substrates topped with an amorphous layer, can be seen in both cases. The formation of amorphous layers is not clear yet, but it could be attributed to the growth conditions and the sample preparation for TEM when exposing to the air.

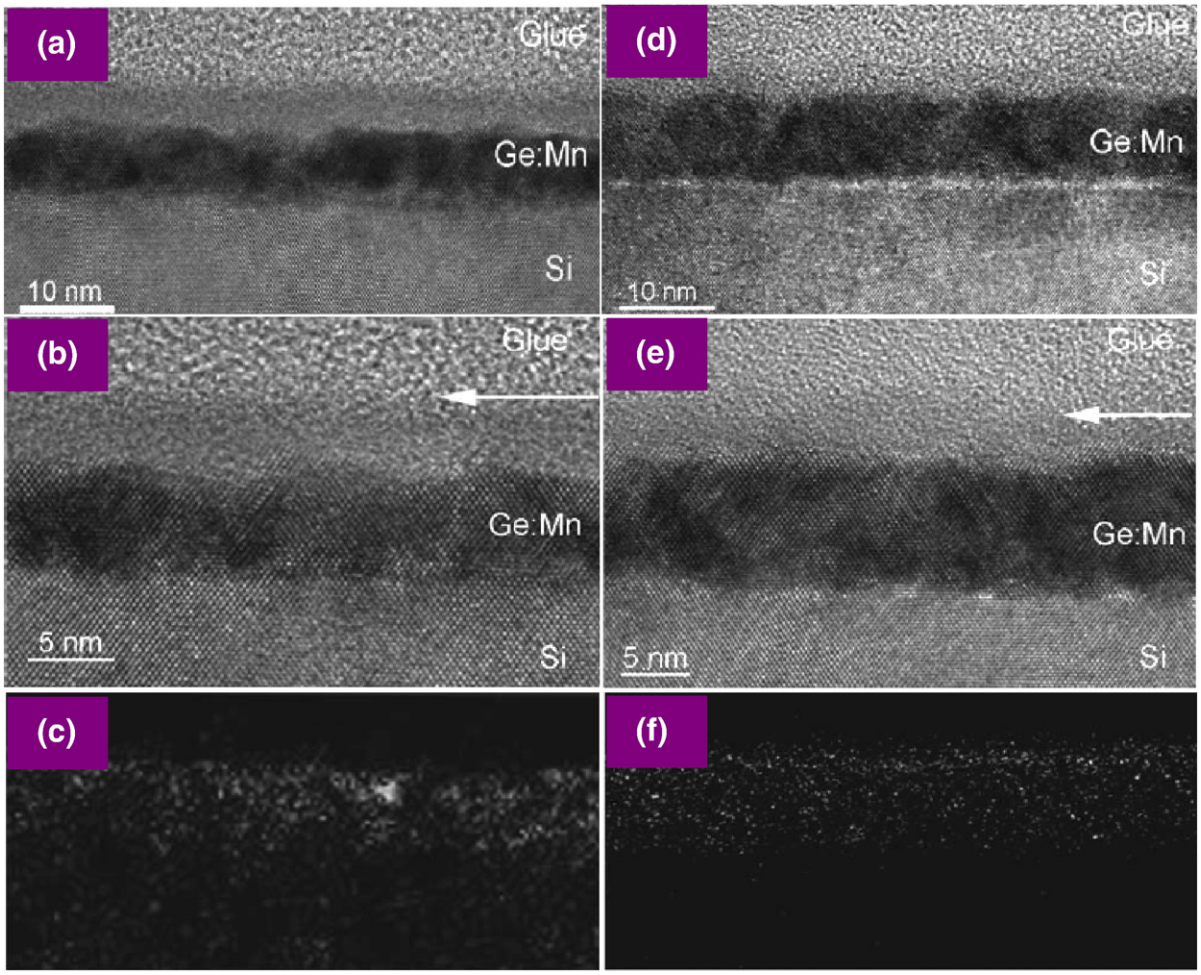

Fig. 4. Typical TEM images of the as-grown (a) and the annealed (d) MnGe thin films with a thickness of 15 nm; the left column is for the as-grown film and the right column is the film after 400 °C annealing. (b) and (e) are the corresponding HR-TEM images of (a) and (d), respectively; (c) and (f) EF-TEM elemental maps of Mn correspond to the regions given by (a) and (d), respectively. The white arrows in (b) and (e) show the separation between the glue and the amorphous MnGe layer.

To understand the structural variation for the two cases, high resolution TEM was carried out and typical <110>zone-axis HR-TEM images are shown in Fig. 4(b) and (e) for the two cases, respectively, where the amorphous layers can be clearly seen. From these HR-TEM images, stacking faults in the crystalline layers can also be seen in both cases. No structural clusters were found through our extensive HR-TEM investigations and no secondary phases were detected by our XRD measurements (not shown here). To further understand the Mn distribution in the MnGe film (crystalline and amorphous), energy filtered TEM was preformed. Fig. 4(c) and (f) give the EF-TEM elemental maps of Mn that correspond to Fig. 4(a) and (d), respectively. It is of interest to note that, in the as-grown case, a higher Mn concentration is found in the amorphous layer when comparing Fig. 4(a) with 4(c). The overall concentration of Mn is low, so that the contrast in the Mn maps tends to be faint. Nevertheless, the distribution of Mn in the entire film can be clearly observed. In contrast, the Mn map (Fig. 4(f)) in the annealed case shows some Mn distribution in the entire film, suggesting that the annealing has not only promoted crystallization, but also redistribute Mn in the entire MnGe film. Nevertheless, a higher Mn concentration can still be observed in the surface region in the annealed sample (refer to Fig. 4 (f)). The fact that, for the as-grown sample, most of Mn was found in the topmost layer suggests that, during the growth of the MnGe film, a dynamic Mn diffusion has taken place, even at a relatively low growth temperature of 250 °C as in our case; Mn tends to diffuse towards the top surface [7].

Fig. 5(a) shows the hysteresis loops at 298 K and 10 K. A clear hysteresis at 298 K indicates room temperature ferromagnetism. Fig. 5(b) shows that the plot of the magnetic moment as a function of temperature at a magnetic field of 100 Oe. The moment in the field cooling (FC) decreases very marginally as the temperature increase from 10 to 298 K, showing that the Curie temperature is above the room temperature. The separation of the zero-field cooling (ZFC) data from that of the field cooling shows the spin glass phase. Before and after annealing, there is no clear difference observed in magnetic properties. The Curie temperature can only be inferred to be above 400 K as shown in Fig. 5(b).

The difference of structural and magnetic properties between the 80 nm-thick and the 15 nm-thick MnGe thin films suggest that when it comes to the nanostructures, the strain, the Mn doping behavior and distribution could be different from that of the bulk films. There might be a threshold thickness for a certain Mn concentration, beyond which the nucleation of metallic clusters (such as Mn_5Ge_3 and $Mn_{11}Ge_8$) takes place and accounts for the RT ferromagnetism ($T_c = 296 \sim 300$ K) [7]. It is therefore of great interest to further investigate MnGe nanostructures to explore their magnetic properties; MnGe nanodots may be formed by ion implantation process of Mn into Ge and by a self-assembling process with a molecular beam epitaxy, as to be discussed next.

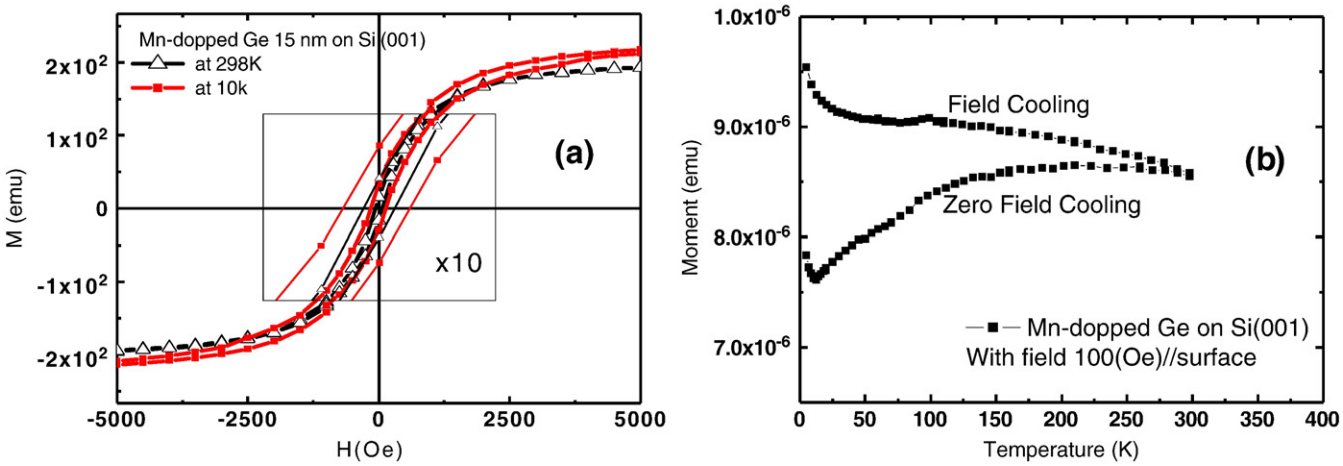

Fig. 5. SQUID measurement of 4% Mn-doped Ge thin film grown on Si with a thickness of 15 nm. (a) hysteresis loops measured at 10 and 298 K; (b) magnetic moment versus temperature measured with a magnetic field of 100 Oe.

4. MnGe nanodots by Mn ion implantation and field controlled ferromagnetism at 10 K

In addition to the efforts of MnGe thin growth, the magnetic properties of Mn_xGe_{1-x} nanostructures by Mn ion implantation into Ge (111) substrates through a patterned SiO_2 as a mask (via diblock copolymer process) have been investigated [20]. Fig. 6(a) shows a SEM image of the SiO_2 pattern on Ge after etching and removing the diblock copolymer layer, showing a regular and repeatable nanohole pattern with a diameter of about 20 nm. The SiO_2 pattern works as a mask for the subsequent uniform implantation of Mn into Ge. Following implantation, rapid thermal annealing was performed on samples at 450 °C in N_2 atmosphere for 20 min, which is an optimum annealing condition as obtained by a series of systematic experiments. During the

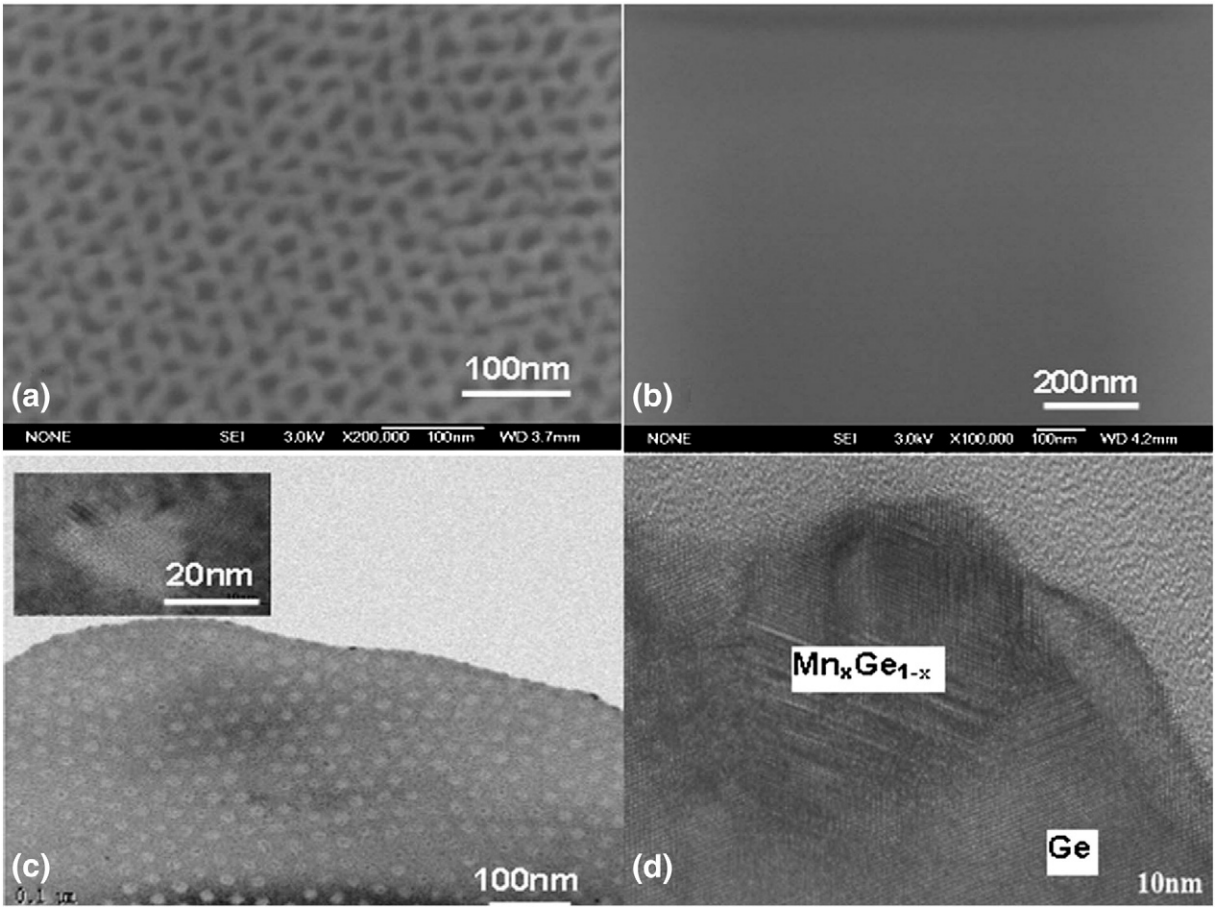

Fig. 6. SEM and TEM micrographs: (a) SEM of the periodic SiO_2 nanostructure mask before Mn implantation showing a regular and repeatable nanohole pattern with a diameter of about 20 nm. (b) SEM of the sample showing a smooth surface after Mn implantation and removal of the SiO_2 mask. (c) TEM planar view of nanostructured MnGe. The inset figure shows enlarged dot planar view with a diameter about 20 nm. (d) TEM cross-section of the nanostructured MnGe.

annealing, a blank Ge wafer was placed on top of the implanted samples to avoid oxidation and other contamination. Fig. 6(b) shows the uniform and smooth surface after removal of the SiO_2. The planar TEM picture of Fig. 6(c) shows that the MnGe nanostructures are well-separated and coherently incorporated in the Ge matrix with an average Mn concentration of about 2%. The inset is the enlarged image of the MnGe nanodots. The cross-section image in Fig. 6(d) shows the detailed structure of a nanodot. The well resolved lattice planes extending throughout the whole image (Fig. 6(d)) reflect the high crystallinity of the layer (also confirmed by the XRD measurements [15]). We can see that the dot sets in a well defined distance from the interface (Fig. 6(d)). A further analysis, however, suggests that some Mn rich phase such as Mn_5Ge_3 was formed in this confined Mn implanted region, where some Mn is presumably to have been accumulated. By calculating the plane distance and angle, we found other phases in addition to the Mn_5Ge_3. Therefore, the MnGe nanostructures via Mn ion implantations show a possible mixture of the MnGe DMS and the metallic clusters, consistent with x-ray diffraction data (not shown here) [15]. Since the average Mn concentration is about 2% only, DMS must be more dilute Mn_xGe_{1-x} ($x<5\%$), i.e., with Mn substitutionals in Ge [15].

Fig. 7 shows the magnetic properties of samples with Mn implantation into Ge via the nano-patterned SiO_2 mask on different doped substrates. It is observed that the Mn implanted p^+ Ge ($10^{19}\,cm^{-3}$) shows stronger ferromagnetic signals than that n-type Ge ($10^{17}\,cm^{-3}$), which may indicate a hole mediated effect. Note that we cannot completely exclude the possibility of the formation of dopant complexes, such as B–Mn and Sb–Mn in the p^+ and n-type Ge, respectively. Taking advantage of this effect, we further fabricated a MOS capacitor device with Mn implanted Ge as the channel layer. Fig. 8 shows the magnetic moment versus applied field for the MOS structure on the n-type substrate under various gate biases at 10 K. When the voltage is applied from −6 to −30 V, the hole concentration in the MnGe channel increases and the magnetic hysteresis becomes larger. At 0 V bias, only a line with a small slope and a small negligible loop are seen; this is because a low density of excess holes is present. When a positive voltage is applied to the gate, holes are partially depleted, resulting in a decrease of the channel magnetization and in the disappearance of magnetic hysteresis. These experimental results demonstrated the hole mediated effect in MnGe, consistent with the finding by Park et al. [3].

5. MnGe self-assembled quantum dots by molecular beam epitaxy (MBE) and field controlled ferromagnetism at 50 K

The research of Mn_xGe_{1-x} nanostructures via Mn ion implantation process has unambiguously demonstrated the modulation of their

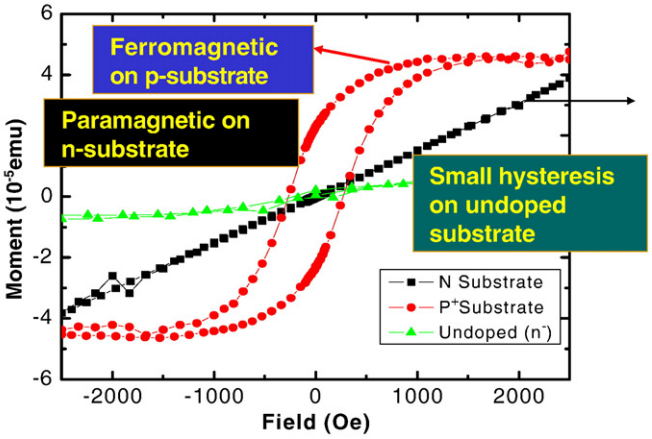

Fig. 7. The magnetic properties of Mn implanted Ge via a nano-patterned SiO_2 mask. The hole mediated effect can be clearly observed in the Mn implanted p-type Ge sample.

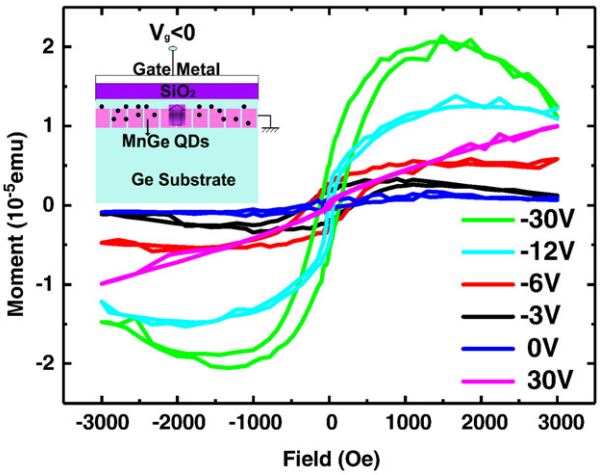

Fig. 8. Magnetic moment vs applied field under various biases from −30 to 30 V at 10 K. The obtained hysteresis is the largest under −30 V gate voltage, and the ferromagnetic phase is turned off under +30 V gate bias. The inset shows the spin gated structure used to investigate C–V and gate bias dependent magnetic properties.

ferromagnetism by applying gate biases in MOS capacitors at a low temperature of 10 K. However, the metallic precipitates such as Mn_5Ge_3 and $Mn_{11}Ge_8$ and implantation damages were found in these nanostructures, which made the system rather complex to understand the contribution of each phase to the hole mediated effect. In addition, the latter makes it difficult to control the process. A possible approach to eliminate the clusters is to use a self-assembled process, which can yield MnGe quantum dots directly on top of Si substrates. Here, we report the successful development of $Mn_{0.05}Ge_{0.95}$ self-assembled quantum dots by molecular beam epitaxy below.

MnGe quantum dots were grown on p-type Si substrates by a solid source MBE system. The Mn and Ge sources were provided by traditional effusion cells. The self-assembled MnGe quantum dots were grown at 450 °C with a Ge growth rate of 0.2 Å/s, similar to the growth of pure Ge quantum dots on Si under a typical Stranski-Krastanow (SK) mode. [21] Cross-section TEM was carried out to determine the structural characteristics and the Mn composition of the $Mn_{0.05}Ge_{0.95}$ quantum dots. It reveals a dome-shape MnGe quantum dot on top of the Si substrate with a Mn diffusion area underneath as shown in Fig. 9(a). The dots have a typical base diameter of about 30 nm and a height of about 8 nm. Electron energy loss spectroscopy (EELS) shows that Mn dopants distribute uniformly inside the quantum dots (Fig. 9(b)). The reddish dots represent Mn atoms. The selected area electron diffraction pattern (SAED) reveals a single crystalline DMS system (Fig. 9(c)). The interface between the dot and the Si substrate shows excellent lattice coherence without any pronounced dislocations or stacking faults (Fig. 9(e)). The energy dispersive X-ray spectroscopy (EDS) further confirms the presence of Mn and Ge inside the MnGe quantum dots.

Metal-oxide-semiconductor capacitors using $Mn_{0.05}Ge_{0.95}$ quantum dots as the channel were fabricated and characterized. Fig. 10(a) shows a schematic drawing of the device structure. Similar to that of the implanted case (Fig. 8, inset), a 40 nm-thick Al_2O_3 was used to minimize the leakage current. Capacitance–voltage curves give a clear transition from an accumulation (of holes) mode under negative bias to a depletion mode under positive bias (not shown here). Significantly, in the depletion mode we observed the decrease of the ferromagnetism of the channel layer via the control of gate voltage at 50 K (Fig. 10(b)). The remnant moments decrease dramatically as the gate bias increases. These experimental data suggest that holes play a significant role in controlling ferromagnetism. By changing the hole concentration in quantum dots, it is possible to manipulate the ferromagnetism in the MnGe DMS system.

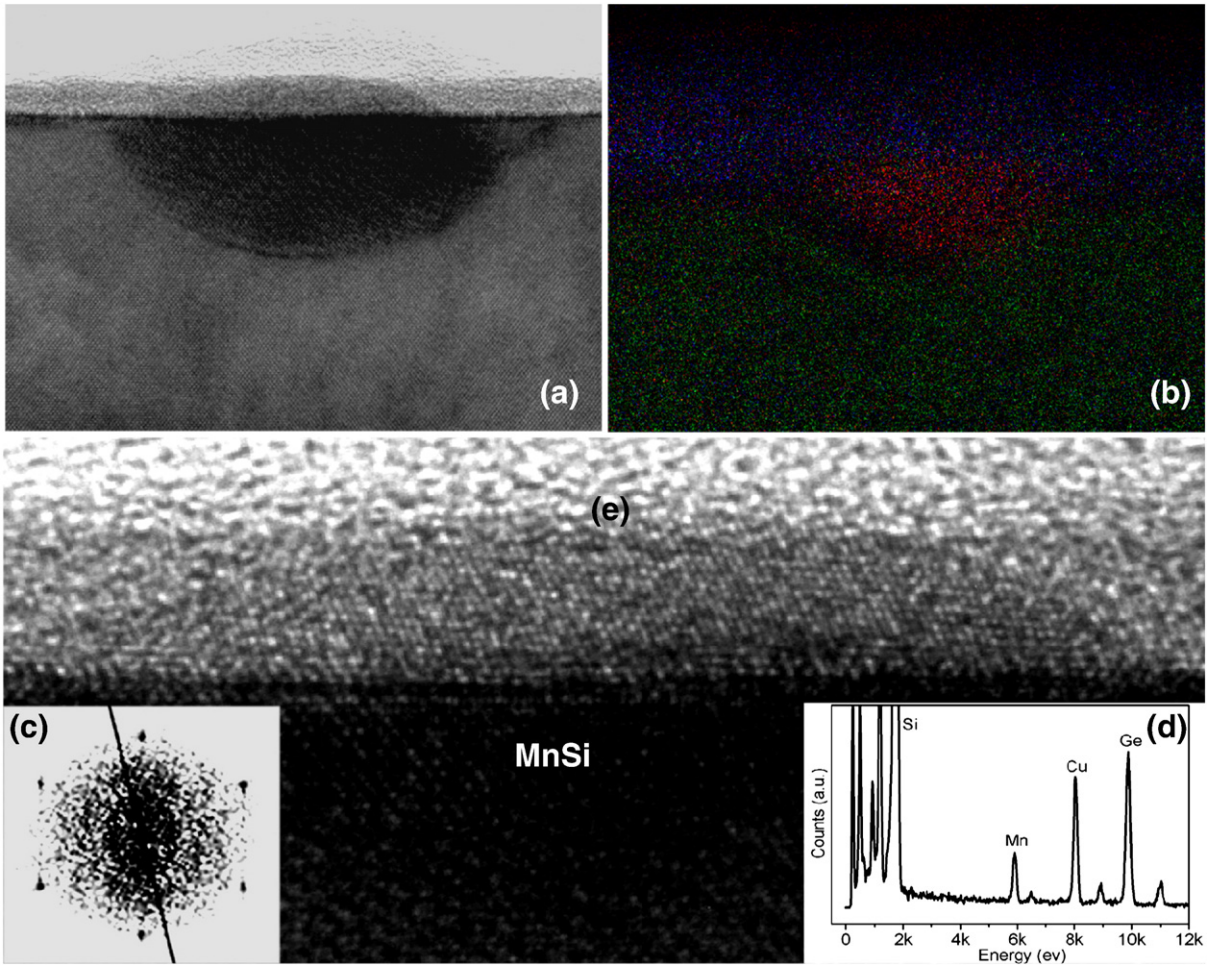

Fig. 9. The structural properties of $Mn_{0.05}Ge_{0.95}$ quantum dots grown on a *p*-type Si substrate. (a) a high resolution TEM cross-section image of a $Mn_{0.05}Ge_{0.95}$ quantum dot. Mn diffuses into the Si substrate, which is shown directly underneath the $Mn_{0.05}Ge_{0.95}$ quantum dot; (b) the EELS composition mapping of Mn distribution; (c) the corresponding SAED pattern of $Mn_{0.05}Ge_{0.95}$ quantum dot, revealing a single crystalline structure; (d) an EDX composition spectrum showing that both Mn and Ge are present in $Mn_{0.05}Ge_{0.95}$ quantum dot; (e) an enlarged HR-TEM image to show the detailed lattice structure of $Mn_{0.05}Ge_{0.95}$ quantum dot.

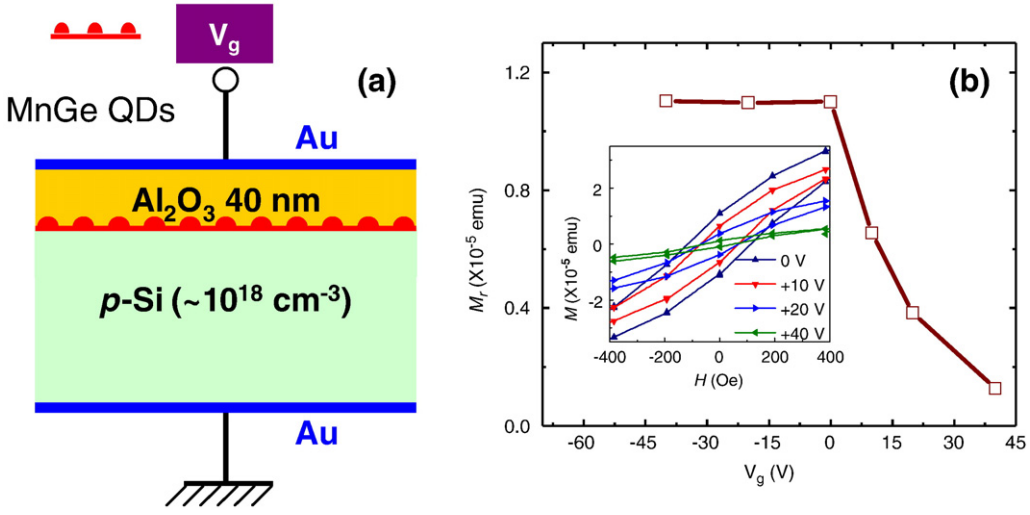

Fig. 10. (a) A schematic drawing of a MOS capacitor using MnGe QDs as the channel layer. During the device operation, the gate was applied with positive and negative biases while the magnetic properties were measured by SQUID; (b) Remnant moments as a function of gate voltage at 50 K.

6. Summary

In summary, with the continuous scaling in the current CMOS technology, future spintronic devices with new functionalities may emerge to resolve, at least in part, the challenges outlined in ITRS. The Mn-doped Ge may emerge as a potential material candidate for various devices because it possesses a strong hole mediated effect. In this paper, we have reviewed the progress of MnGe thin films and

MnGe nanostructures. The approach of using nanostructures appears to be rather promising to produce designed DMS materials. The more recent results of electric field manipulation of MOS structures fabricated from a self-assembled DMS quantum dots by MBE demonstrated a major step forward in the quest of low power spintronic devices. With further understanding and continuous efforts on the MnGe materials and devices, the MnGe based Spin-FETs may become a viable technology for magnetoelectronics.

Acknowledgements

This research was in part supported by SRC, Marco, NERC, ARO, DARPA, and sponsoring industrial companies through WIN and FENA. We also want to acknowledge our collaborators Dr. Yong Wang and Professor Jin Zou from the University of Queensland for the TEM experiments.

References

[1] http://www.itrs.net/Links/2007ITRS/Home2007.htm.
[2] O. Masaaki, et al., Mn distribution behaviors and magnetic properties of GeMn films grown on Si (001) substrates, J. Crystal Growth 311 (2009) 2147.
[3] Park Y.D , et al., A group-IV ferromagnetic semiconductor Mn_xGe_{1-x}, Science 295 (2002) 651.
[4] S. Cho, et al., Ferromagnetism in Mn-doped Ge, Phys. Rev. B 66 (2002) 033303.
[5] M. Jamet, et al., High-Curie-temperature ferromagnetism in self-organized $Ge_{1-x}Mn_x$ nanocolumns, Nat. Mater. 5 (2006) 653.
[6] S. Ahlers, et al., Magnetic and structural properties of Ge_xMn_{1-x} films: precipitation of intermetallic nanomagnets, Phys. Rev. B: Condens. Matter 74 (2006) 214411.
[7] Y. Wang, et al., Mn behavior in $Ge_{0.96}Mn_{0.04}$ magnetic thin films grown on Si, J. Appl. Phys. 103 (2008) 066104.
[8] Y. Wang, et al., Direct structural evidences of $Mn_{11}Ge_8$ and Mn_5Ge_2 clusters in $Ge_{0.96}Mn_{0.04}$ thin films, Appl. Phys. Lett. 92 (2008) 101913.
[9] L. Ottaviano, et al., Phase separation and dilution in implanted Mn_xGe_{1-x} alloys, Appl. Phys. Lett. 88 (2006) 061907.
[10] M. Passacantando, et al., Growth of ferromagnetic nanoparticles in a diluted magnetic semiconductor obtained by Mn^+ implantation on Ge single crystals, Phys. Rev. B: Condens. Matter. 73 (2006) 195207.
[11] S. Picozzi, et al., X-ray absorption spectroscopy in Mn_xGe_{1-x} diluted magnetic semiconductor: experiment and theory, Appl. Phys. Lett. 86 (2005) 062501.
[12] Y.J. Cho, et al., Ferromagnetic $Ge_{1-x}M_x$ (M = Mn, Fe, and Co) nanowires, Chem. Mater. 20 (2008) 4694–4702.
[13] M.I. Meulen, et al., Single crystalline $Ge_{1-x}Mn_x$ nanowires as building blocks for nanoelectronics, Nano Lett. 9 (2009) 50–56.
[14] I.T. Yoon, et al., Ferromagnetism in self-assembled Ge quantum dots material followed by Mn-implantation and annealing, Solid State Electronics 52 (2008) 871–876.
[15] J. Chen, K.L. Wang, K. Galatsis, Electrical field control magnetic phase transition in nanostructured MnGe, Appl. Phys. Lett. 90 (2007) 012501.
[16] A.P. Li, et al., Magnetism in Mn_xGe_{1-x} semiconductors mediated by impurity band carriers, Phys. Rev. B: Condens. Matter. 72 (2005) 195205.
[17] A.P. Li, et al., Dopant segregation and giant magnetoresistance in manganese-doped germanium, Phys. Rev. B 75 (2007) 201201.
[18] Bougeard, et al., Clustering in precipitate-free MnGe magnetic semiconductor, Phys. Rev. Lett. 97 (2006) 237202.
[19] H. Li, et al., Magnetic and electrical transport properties of $Ge_{1-x}Mn_x$ thin films, J. Appl. Phys. 100 (2006) 103908.
[20] S.H. Kim, et al., Highly oriented and ordered arrays from block copolymers via solvent evaporation, Adv. Mater. 16 (2004) 226.
[21] J.L. Liu, S. Tong, K.L. Wang, Self-assembled Ge quantum dots on Si and their optoelectronic devices, in: A.A. Balandin, K.L. Wang (Eds.), Handbook of Semiconductor Nanostructure and Devices, 3 volumes, vol.1, American Scientific Publishers, Los Angeles, California, USA, 2006, pp. 1–32.